https://doi.org/10.1016/j.vacuum.2018.03.024

Effect of post-annealing on laser-ablation deposited WS_2 thin films

H. Wang[1], S.M. Ng[1], H.F. Wong[1], W.C. Wong[1], K.K. Lam[1], Y.K. Liu[1], L.F. Fei[1], Y.B. Zhou[2], C.L. Mak[1], Y. Wang[2], C.W. Leung[1,*]

[1]Department of Applied Physics, The Hong Kong Polytechnic University, Hung Hom, Hong Kong SAR, China

[2]School of Materials Science and Engineering, Nanchang University, Nanchang, Jiangxi 330031, China

Tel: +852-2766-5670, Email: dennis.leung@polyu.edu.hk

We deposited WS_2 thin films by pulsed laser deposition on sapphire substrates at room temperature, and studied the effect of post-annealing temperature on the quality of the WS_2 films. By comparing the full-width-at-half-maximum of the characteristic WS_2 Raman peaks, we explored the relationship between the post-annealing temperature and the crystallinity of WS_2 films. The optoelectronic measurements conducted on post-annealed WS_2 film-based photodetectors showed improvement with rising annealing temperatures. Our study revealed the possibility of preparing large-area dichalcogenides for optoelectronic applications.

Key words: pulsed laser deposition, post-annealing, Raman spectroscopy, WS_2

Introduction

Layered transition metal dichalcogenides (TMDs) such as MoS_2 and WS_2 have attracted a lot of attention due to their exotic properties, such as indirect bandgap-to-direct bandgap transition, spin-orbit-induced electronic-band splitting, and spin-valley coupling [1,2,3]. Typically, TMDs are prepared by chemical vapor deposition (CVD) [4,5,6] and mechanical exfoliation [7,8], but these methods suffer from drawbacks such as limited control over size, the need of suitable precursor materials, elevated growth temperatures and prolonged growth time.

Physical vapor deposition has the advantage of preparing ultrathin layers of materials with high uniformity. In particular, pulsed laser deposition (PLD) has been generally deployed in the fabrication of complex materials for retaining the stoichiometry of the resultant thin films. Reported PLD preparation of WS_2 thin films were conducted in sulphur-abundant conditions at around 350°C [9,10]. It was also reported that post-annealing after the deposition process can influence the crystallinity of the resultant films [11]. Based on these, we studied the effect of post-annealing on room temperature (RT)-deposited WS_2 thin films systematically. Besides, their optoelectronic performances were also investigated. Our study sheds light on the PLD preparation of large-area WS_2 samples, which can have potential for device applications.

Experimental details

WS_2 film deposition. WS_2 films were produced by PLD on 1 mm-thick sapphire (0001) substrates of area 5×5 mm^2 at RT, by ablating a WS_2 target (99.99% purity) using a KrF excimer pulsed laser source (wavelength = 248 nm). The pulse repetition rate and power were

1 Hz and 250 mJ. The chamber was pumped down to 2×10^{-4} Pa before deposition. The thickness of the deposited WS_2 films was 12 nm as determined by atomic force microscopy. In order to improve the crystallinity of the WS_2 layer, the films were post-annealed at fixed temperatures in a rapid thermal processor (RTP) with flowing nitrogen at atmospheric pressure for 20 min, and then cooled down to RT naturally to complete the annealing process. Raman spectra of the WS_2 thin films were obtained using a laser source of wavelength 488 nm.

Device fabrication. Au electrodes of area 60×450 μm^2 were deposited on top of the WS_2 films with sapphire substrates by electron beam (e-beam) evaporation, using a stainless steel shadow mask to define the channels (channel length = 100 μm and channel width = 450 μm) for photoelectrical measurements. We used a blue LED of wavelength 452.5 nm for photo-excitation, with a uniform sample illumination of intensity between 0.1 to 200 mW-cm^{-2} over the channel region. Electrical measurements were performed at RT using a Keithley 2400 sourcemeter and a Keithley 6487 picoammeter.

Results and discussions

The Raman spectra of the WS_2 films before and after annealing are presented in Fig. 1. As shown in Fig. 1(a), the as-deposited WS_2 film without undergoing annealing process (Sample I) shows no Raman signal. After post-annealing the film *ex-situ* at 610°C in a nitrogen flow for 20 min, two characteristic WS_2 peaks are observed from the film (Sample III). For comparison, we also measured the Raman spectrum of WS_2 film deposited at 300°C but without undergoing post-annealing (Sample II). It is noticed that the peak intensities of 610°C post-annealed WS_2 film are much stronger than those from WS_2 film deposited at 300°C but without post-annealing, implying a higher quality for the WS_2 film which has undergone

post-annealing.

As previously reported, there are two characteristic Raman peaks for WS_2, namely the in-plane vibration peak (E^1_{2g}) at 356.7 cm^{-1} and the out-of-plane vibration peak (A_{1g}) at 421.0 cm^{-1} [6,8,11]. The E^1_{2g} and A_{1g} peaks are both observed in WS_2 films deposited at high temperature without post-annealing (Fig. 1(a)), and in RT-deposited samples which have undergone post-annealing (from 310°C to 610°C, Fig. 1(b)). The separation between the two peaks is 64.2 cm^{-1} for all the samples, implying a multilayered structure of WS_2 films. Also, there is no obvious shift of the two peaks among samples post-annealed under different temperatures.

Fig. 1 (c) summarizes the change in the full-width at half-maximum (FWHM) of the characteristic Raman peaks in the WS_2 films shown in Fig. 1(b), as a function of the post-annealing temperature. Generally, the FWHM of WS_2 films is found to decrease with increasing annealing temperature. This result indicates the WS_2 film crystallinity can be improved by RTP treatment. Such an improvement can be attributed to the recrystallization process [12]: by the RTP treatment the nanocrystalline flakes could be reorganized to form larger flakes.

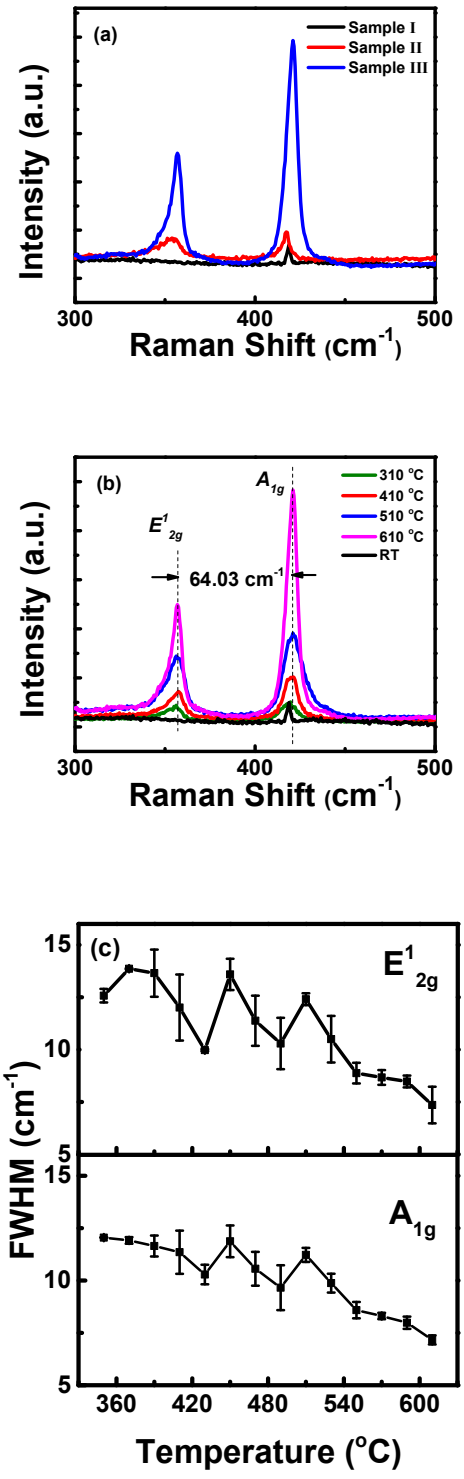

Fig. 1 Raman spectra of WS_2 films. (a) comparison between samples deposited at RT (I and III) and at 300°C (II), with sample III underwent post-annealing (at 610°C) while others did not. (b) Raman spectra of RT-deposited WS_2 samples post-annealed at different temperatures. (c) Relationship between post-annealing temperature and the FWHM of E^1_{2g} and A_{1g} Raman peaks.

It is interesting to correlate the observed improvement of film microstructure to the performance of WS_2 in fabricated devices for specific applications. To this end, we tested the effect of post-annealing on WS_2 films' photoelectrical properties. Photoelectric performances of the post-annealed films were tested using the device geometry shown in Fig. 2(a), which consists of Au electrodes evaporated on as-deposited WS_2 films as described in the experimental section. Table 1 lists the dark current of WS_2 photodetectors prepared with films post-annealed at different temperatures, under an applied bias (V_{ds}) of +5 V. When the post-annealing temperature increases from 310°C to 610°C, the device dark current rises from 3.6×10^{-10}A to 1.24×10^{-4} A.

Fig. 2(b) shows the current-voltage ($I - V$) curves of WS_2 films post-annealed at different temperatures and measured with a light intensity of 160 mW-cm^{-2}. The measurements were done by sweeping the applied voltage between ±5 V. The linear and symmetric $I - V$ traces for small bias voltages indicate Ohmic contacts between the WS_2 channel and the Au electrodes. At the same V_{ds}, the photocurrent increases with rising post-annealing temperature of the WS_2 film. The better conducting performance and higher photo-generated current can be attributed to the better crystallinity of the films annealed at higher temperatures.

To understand how the post-annealing temperature and the light power affects the photo-generated current, $I-V$ measurements were carried on the devices under different illumination intensities. Fig. 2(c) shows the dependence of the photocurrent with the incident light intensity. Generally, the photocurrent rises with increasing light intensity as expected. Besides, the photocurrent is larger under identical illumination for samples annealed at higher temperatures. The slope of the log-plots in Fig. 2(c) can be fitted by the power law $I = kP^{\alpha}$, where I and P correspond to the photocurrent and incident light intensity, and k is a constant [14]. The fitted values of α for samples annealed at different temperatures are listed in Table 2. A non-unity value of α is caused by the complex processes of electron-hole generation,

trapping, and recombination resulting from defects or charge impurities within the semiconductor [15, 16] The increasing value of α with rising annealing temperature therefore implies an improved WS_2 crystallinity, which is consistent with the decreasing FWHM of Raman peaks as shown in Fig. 1(c)).

Important optoelectronic properties such as photoresponsivity (R), detectivity (D^*), and external quantum efficiency (EQE) of photodetectors were also studied for evaluating the device performance. Photoresponsivity is a measure of the device electrical response to incident light and is defined as $R = \frac{I}{AP}$, where A is the effective area of the detector. The annealing temperature-dependent responsivity of the WS_2 devices is displayed in Fig. 2(d), under an incident power density of 160 mW-cm^{-2}. R is found to be higher for WS_2 films annealed at higher temperatures. For example, the largest R value under a 5 V bias is 0.001 AW^{-1} for device with WS_2 annealed at 310°C, as compared with 0.18 AW^{-1} for WS_2 annealed at 610°C [17].

Temperature (°C)	310	410	510	610
Dark current (A)	3.6×10^{-10}	4.52×10^{-7}	8.16×10^{-5}	1.24×10^{-4}

Table 1 Dark current for WS_2 samples post-annealed at different temperatures (V_{ds} = 5 V).

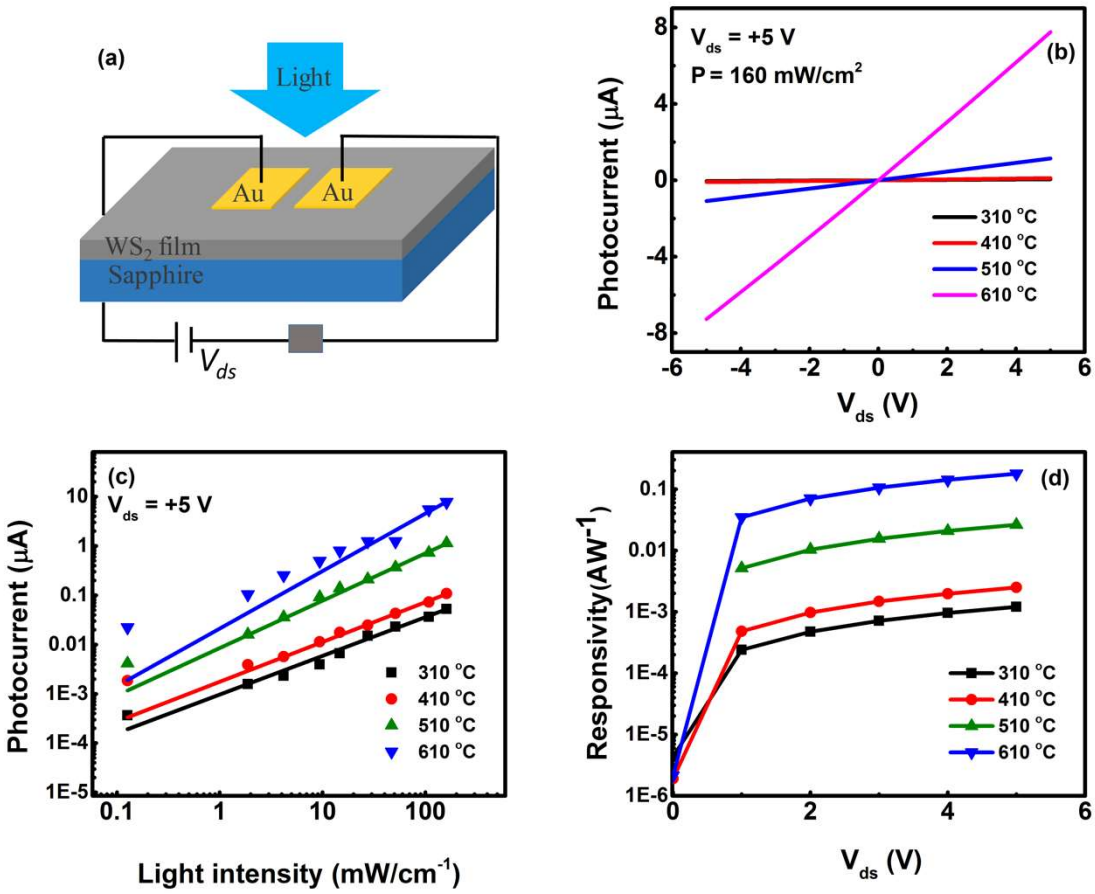

Fig. 2 Photodetector device measurements based on PLD and post-annealed WS_2 films. (a) Schematic of photodetector structure, with the LED light applied normal to the film. (b) to (d) shows the measurement results for photodetectors with WS_2 post-annealed at different temperatures, including current–voltage plots obtained in the presence of laser (b), photocurrent vs. light intensity (c) and responsivity as a function of V_{ds}.

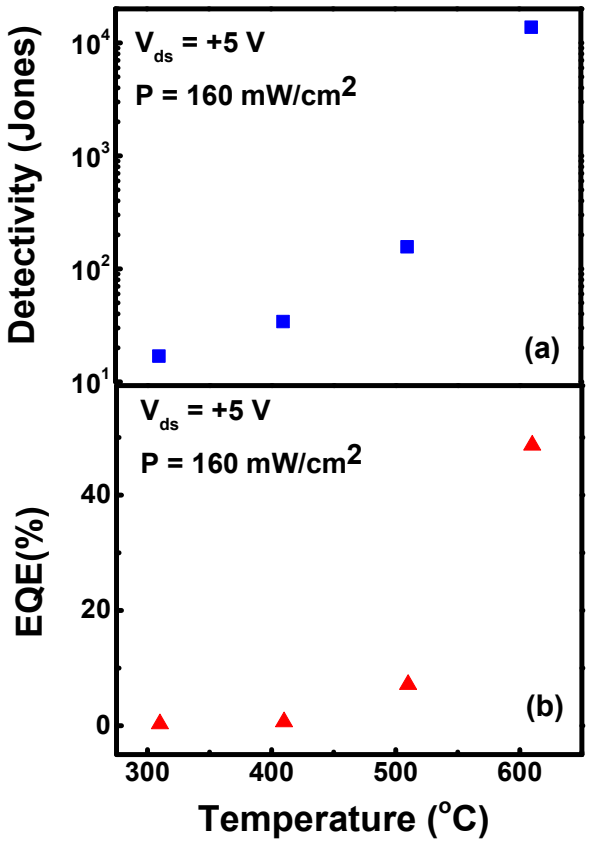

Fig. 3 Dependence of detectivity (a) and *EQE* (b) on WS_2 post-annealing temperatures.

Annealing temperature (°C)	310	410	510	610
α	0.78	0.81	0.96	1.16

Table 2 Values of α in equation $I = kP^{\alpha}$ for WS_2 post-annealed at different temperatures.

In photodetector investigations, the specific detectivity (D) is typically used as the figure of merit for device performance. By assuming that shot noise from dark current constitutes a major contribution to the total noise, D can be defined as $\boldsymbol{D}= \frac{RA^{1/2}}{(2eI_{dark})^{1/2}}$, where e is the

electron charge and I_{dark} is the dark current. The correlation between D and WS_2 post-annealing temperature is shown in Fig. 3(a). With the increase of the annealing temperature, there is an improvement of the crystallinity of the samples and hence enhanced charge carrier lifetime and reduced electron-hole recombination [18]. These result in a strong increase in R and D, despite the rise of I_{dark} with increasing sample annealing temperature. At an incident light intensity of 160 mW-cm^{-2}, there is a change of D by 3 orders of magnitude, as the WS_2 post-annealing temperature changes from 310°C to 610 °C [14]. Finally, EQE is the number of photo-induced carriers that are detected per incident photon. It is defined by the equation $EQE = \frac{hcR}{e\lambda}$, where h is Planck constant, c is the velocity of light, and λ is the incident wavelength [19]. The variation of EQE with the post-annealing temperature is illustrated in Fig. 3(b). Again the EQE has shown significant improvement with the rising annealing temperatures, which can also be explained by the reduced carrier recombination due to an improved sample crystallinity with rising annealing temperature, that has led to an improved R and hence the EQE value.

Conclusions

We studied the effect of post-annealing on WS_2 films deposited by pulsed laser deposition at room temperature on sapphire substrates. Raman spectra on the samples have shown improved WS_2 film qualities with the post-annealing process. Photodetection studies based on the post-annealed samples have shown strong correlations between the post-annealing temperature and the photodetection responses. Our studies have shown the potential of PLD-deposited WS_2 thin films in photodetection applications, and has identified a simple route for improving the quality of the WS_2 films for achieving better photodetection performances.

Acknowledgement

Financial support by PolyU (G-YBJ1, G-YBPU, 1-ZE25, 1-ZVGH) and UGC, HKSAR (PolyU 153015/14P) are acknowledged.

References

[1] Z. Y. Zhu, Y. C. Cheng, U. Schwingenschlögl, Giant spin-orbit-induced spin splitting in two-dimensional transition-metal dichalcogenide semiconductors, Phys. Rev. B. 84 (2011) 153402.

[2] W. J. Zhao, Z. Ghorannevis, L. Chu, M. L. Toh, C. Kloc, P. H. Tan, G. Eda, Evolution of Electronic Structure in Atomically Thin Sheets of WS_2 and WSe_2, ACS Nano. 7 (2013) 791-797.

[3] D. Xiao, G. B. Liu, W. X. Feng, X. D. Xu, W. Yao, Coupled Spin and Valley Physics in Monolayers of MoS_2 and Other Group-VI Dichalcogenides, Phys. Rev. Lett. 108 (2012) 196802.

[4] S. Tongay, W. Fan, J. Kang, J. Park, U. Koldemir, J. Suh, D. S. Narang, K. Liu, J. Ji, J. Li, R. Sinclair, J. Wu, Tuning Interlayer Coupling in Large-Area Heterostructures with CVD-Grown MoS_2 and WS_2 Monolayers, Nano Lett. 14 (2014), 3185–3190.

[5] T. Georgious, R. Jalil, B. D. Belle, L. Britnell, R. V. Gorbachev, S. V. Morozov, Y. J. Kim, S. J. Haigh, O. Makarovsky, L. Eaves, L. A. Ponomarenko, A. K. Geim, K. S. Novoselov, A. Mishchenko, Vertical field-effect transistor based on graphene–WS_2 heterostructures for flexible and transparent electronics, Nat. Nanotech. 8 (2013) 100–103.

[6] N. Perea-Lopez, A. L. Elías, A. Berkdemir, A. Castro-Beltran , H. R. Gutiérrez, S. Feng, R. Lv, T. Hayashi, F. López-Urías, S. Ghosh, B. Muchharia, S. Talapatra, H. Terrones, M. Terrones, Photosensor Device Based on Few-Layered WS_2 Films, Adv. Funct. Mater. 23 (2013) 5511-5517.

[7] D. Viory, H. Yamaguchi, J. Li, R. Silva, D. C. B. Alves, T. Fujita, M. Chen, T. Asefa, V.

B. Shenoy, G. Eda, M. Chhowalla, Nat. Mater. 12 (2013) 850–855.

[8] H. S. S. Ramakrishna Matte, A. Gomathi, A. K. Manna, D. J. Late, R. Datta, S.K. Pati, C.N.R. Rao, MoS_2 and WS_2 Analogues of Graphene Angew. Chem. Int. Ed. 49 (2010) 4059-4062.

[9] J. D. Yao, Z. Q. Zheng, J. M. Shao, G. W. Yang, Stable, highly-responsive and broadband photodetection based on large-area multilayered WS_2 films grown by pulsed-laser deposition, Nanoscale 7 (2015) 14974-14981.

[10] T. A. J. Loh, D. H. Chua, A. T. S. Wee, One-step Synthesis of Few-layer WS_2 by Pulsed Laser Deposition, Sci Rep. 5 (2015) 18116.

[11] L. Cheng, W. Huang, Q. Gong, C. Liu, Z. Liu, Y. Li, H. Dai, Ultrathin WS_2 Nanoflakes as a High-Performance Electrocatalyst for the Hydrogen Evolution Reaction, Angew. Chem. Int. Ed. 53 (2014) 7860-7863.

[12] J.W. Chung, Z. R. Dai, F. S. Ohuchi, WS_2 thin films by metal organic chemical vapor deposition, J. Cryst. Growth 186 (1998) 137-150.

[13] K. Shirai, Y. Moriguch., M. Ichimura, A. Usami, M. Saji, Relationship between Raman Spectra and Crystallinity of CdS Films Grown by Cathodic Electrodeposition, Jpn. J. Appl. Phys. 35 (1996) 2057-2060.

[14] L. Zeng, L. Tao, C. Tang, B. Zhou, H. Long, Y. Chai, S. P. Lau, Y. H. Tsang, High-responsivity UV-Vis photodetector based on transferable WS_2 film deposited by magnetron sputtering, Sci. Rep. 6 (2016) 20343.

[15] X. Zhou, L. Gan, W. Tian, Q. Zhang, S. Jin, H. Li, Y. Bando, D. Golberg, T. Zhai, Ultrathin $SnSe_2$ Flakes Grown by Chemical Vapor Deposition for High-Performance Photodetectors, Adv. Mater. 27 (2015) 8035–8041.

[16] Z. Q. Zheng, J. D. Yao and G. W. Yang, Growth of centimeter-scale high-quality In_2Se_3 films for transparent, flexible and high performance photodetectors, J. Mater. Chem. C 4 (2016) 8094-8103.

[17] H. Tan, Y. Fan, Y. Zhou, Q. Chen, W. Xu, J. H. Warner, Ultrathin 2D Photodetectors Utilizing Chemical Vapor Deposition Grown WS_2 with Graphene Electrodes, ACS Nano. 10 (2016) 7866-7873.

[18] A. G. Ardakani, M. Pazoki, S.M. Mahdavi, A. R. Bahrampour, N. Taghavinia, Ultraviolet photodetectors based on ZnO sheets: The effect of sheet size on photoresponse properties, Appl. Surf. Sci. 258 (2012) 5405 - 5411.

[19] C. Zhang, S. Wang, L. Yang, Y. Liu, T. Xu, Z. Ning, A. Zak, Z. Zhang, R. Tenne, Q. Chen, High-performance photodetectors for visible and near-infrared lights based on individual WS_2 nanotubes, Appl. Phys. Lett. 100 (2012) 243101.